Surface Review and Letters, Vol. 2, No. 6 (1995) 731–739

ATOMIC STRUCTURE OF THE Si(100)-(5×3)–Au SURFACE

G. JAYARAM and L. D. MARKS
Department of Materials Science and Engineering, Northwestern University, Evanston, IL 60208, USA

Received 27 June 1995

An atomic structure model for the 5 × 3 phase observed on annealing Au deposited on clean Si(100) surfaces at room temperature is proposed from an ultrahigh-vacuum transmission electron microscopy imaging and diffraction study. The basic structure is made of silicon and gold atoms arranged in four parallel rows on the surface, and two parallel rows of gold atoms in the third layer in the bulk. The spacing between these subsurface gold rows results in the application of a compressive strain to the two outer surface rows. A combination of such structural units arranged in 5 × 3 and $\sqrt{26} \times 3$ geometries satisfactorily explains earlier scanning tunneling microscopy, and current transmission electron microscopy data.

1. Introduction

Interfaces in metal–semiconductor systems play a critical role in determining the electronic properties of devices and a detailed characterization of the interfacial microstructure and chemistry in these systems is therefore essential. Of practical importance, for example, is the issue of alloy formation on metal deposition at room temperature, while an issue more fundamental in interest is the microstructure that results on annealing such metal–semiconductor interfaces.

In this regard, the Au–Si(100) interface is an interesting and important system for study, since controversies surround both the room-temperature and annealing behavior. Studies characterizing room-temperature metal deposition typically seek to address such issues as the formation of an alloy, the critical thickness of Au required to initiate this reaction, and the mechanism by which such a reaction proceeds. It is now generally agreed that Au deposition on clean Si(100)-(2 × 1) surfaces results in the formation of an alloy above a certain critical thickness.[1–4] There is, however, little agreement over this value and in fact, values span the submonolayer, e.g., 0.33 ML[1] or 0.5 ML,[2] to a few monolayers, e.g., about 2–4 ML.[3,4] Low-energy electron diffraction (LEED) studies[2,5–8] report that, in the very initial stages of Au deposition, the Si(100)-(2 × 1) spots weaken in intensity and finally disappear, leaving behind a 1×1 surface. Real-space STM measurements,[8] in this deposition regime, reveal regions to be locally ordered: Au atoms are reported to form dimers and grow as two-dimensional layers in a local 2 × 2 structure with further Au deposition resulting in the appearance of the 1 × 1 structure as reported by LEED. At much higher coverages, i.e., 3 nm, a weak diffuse ring of gold–silicide, which sharpened into spots on increased deposition is observed.[16]

The annealing behavior of the system has been studied primarily using LEED.[5–7,9] These studies reveal a variety of surface reconstructuions for the system, depending on the Au coverage and annealing temperature. For example, a 5 × 1 structure,[7,9] and a c(8 × 2)-type pattern that transforms to a $\sqrt{26} \times 1$ (along with 1/3 order streaks) or a $\sqrt{26} \times 3$ (along with 1/2 order streaks) structure[5,6] have all been reported. In fact, a schematic phase map for the appearance of the different reconstructions as a function of coverage and annealing temperature was even proposed in one of these studies.[6]

One of the drawbacks, however, of gleaning information about the real-space structure from periodicities in diffraction data is that the latter are averaged over the region of the probe. This was amply illustrated by STM–LEED studies of both room-temperature[8] and annealing behavior;[10] these, to

our knowledge, are the only studies to date that combine reciprocal-space data with real-space structure information. The latter study shows that the $\sqrt{26}\times 3$ structure reported by earlier LEED investigations[5,6] actually corresponds to a mixture of 5×3 and $\sqrt{26}\times 3$ units in real space.

The main feature seen in the images of these two structures was the presence of *stripes* running along the $\langle 1\bar{1}0\rangle$ directions with an interstripe spacing of 5α, where α represents the spacing between the (110) planes in bulk silicon. Each stripe contained four parallel rows with atomic scale features of two different sizes called A and B, while others had in addition, a lower density of some very bright features called C. These stripes were labeled type (i) and type (ii) respectively. Every fifth row on the surface was missing, resulting in a *trench* separating adjacent stripes. Features of the same type were spaced 3α apart in the direction parallel to the stripe, and the arrangement of the stripes determined either a 5 or a $\sqrt{26}$ periodicity in the orthogonal direction, i.e., the 5×3 unit resulted from adjacent type (i) stripes, while a phase slip of 1α due to the presence of a type (ii) stripe in between two type (i) stripes caused the $\sqrt{26}\times 3$ structure. The outermost rows on the stripes were also reported to move in towards the center, with the inner two rows staying in bulk locations, resulting in a 17% compression. Although the images were unable to reveal conclusively the chemical identity of the features on the stripes or inside the trenches (i.e., Au or Si), using x-ray photoelectron spectroscopy (XPS) a maximum limit of 0.7 ML was suggested for Au that could remain in the first four layers in a 5×3 structure. This is in disagreement with Rutherford backscattering spectroscopy data[9] which placed the value at 1.7 ML for a 5×1 surface.

In this paper, we report results using a combination of high-resolution transmission electron microscopy imaging (HREM) and diffraction techniques on the annealing behavior of Au deposited on clean Si(100) surfaces at room temperature. The focal points of the study were to gain an understanding of the reconstruction periodicity and distribution of the species, in real space. The paper is organized in the following manner. Surface preparation details are presented in Sec. 2 followed by a description of the experimental imaging and diffraction data in Sec. 3. Data analyses (and the structure model arising from such analyses) are explained in Sec. 4 and the underlying mechanism resulting in the structure is discussed in Sec. 5.

2. Experimental Procedure

Thin samples of p-type Si(100) (B doped at 1 ohm-cm) were mechanically polished, slightly dimpled, and chemically thinned to electron transparency in a 10% HF + 90% HNO_3 solution before transfer into an ultrahigh-vacuum surface-science chamber (UHV–SSC) attached to a Hitachi UHV-H9000 electron microscope[11] (working vacuum of 7×10^{-11} Torr in both chambers). Sample preparation inside the UHV–SSC involved a cyclic combination of 2.5-kV Ar^+ sputtering and electron-beam annealing cycles until clean Si(100) surfaces were obtained; such surfaces were characterized by the appearance of the (2×1)-type reconstruction spots in the transmission electron diffraction (TED) patterns.[12]

Evaporator filaments in the UHV–SSC were outgassed and Au was deposited onto clean surfaces held at room temperature; the thickness of the deposited film was estimated using a quartz-crystal monitor. The sample was then annealed and transferred into the microscope under UHV conditions. TED patterns and HREM images of the system were recorded at microscope operating voltages of 300 kV [radiation damage was not an issue, unlike the Si(111)-(5×2)–Au system[13]]. After each observation, the sample was ion milled and annealed to establish a clean substrate surface prior to any further deposition; sample cleanliness was carefully monitored before and after each deposition cycle using parallel electron energy-loss spectroscopy. The results reported below are from numerous such cycles.

3. Results

We will present here the electron diffraction and high-resolution microscopy data, and pull these together to yield the structure model in the next section.

3.1. *TED data*

3.1.1. *Room-temperature behavior*

TED patterns following room-temperature deposition showed features consistent with those reported

by earlier diffraction studies.[2,5–7] At the initial stages of deposition, only a decrease in the intensity of the Si-surface spots was observed. These spots disappeared, leaving behind a 1 × 1 surface and a diffuse ring which sharpened considerably as the coverage was increased to roughly 3 ML [1 ML of Si on a (100) surface = 6.8×10^{14} atoms/cm^2]. Although the ring spacing suggested formation of a gold–silicide compound, lack of surface-spectroscopy data precludes us from commenting further on this issue.

3.1.2. *Annealing behavior*

A TED pattern obtained on annealing the surface (with ~ 3 ML gold) is shown in Fig. 1. One-fifth-order spots and weak one-half-order streaks are seen along the two (110) directions. Strong intensity of the eight sets of spot pairs and the 1,6/5 type spots are the other noticeable features in the patterns; one such spot pair and a 1,6/5 spot are labeled as A and B respectively in the figure. These spot pairs did not always co-exist with the reconstruction spots and were found to vary in intensity as a function of processing conditions. While numerous hypotheses can be advanced to explain the origin of these features in the TED patterns, a better understanding can be obtained from real-space HREM data, as explained below.

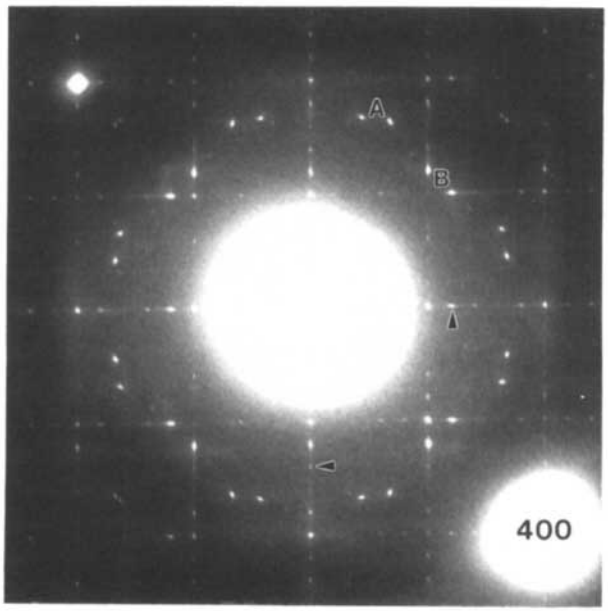

Fig. 1. A typical diffraction pattern obtained following an anneal of the Au–Si(100) surface; reconstruction spots are arrowed. Weak "1/2"-order streaks, eight spot pairs and strong intensity in the 1,6/5 type spots are the other prominent diffraction features. A spot pair is denoted by A while B denotes a 1,6/5 type spot.

3.2. *HREM imaging and processing*

A series of through-focal HREM images were collected, digitized using an Optronics P1000 microdensitometer, and analyzed using SEMPER software. Although the images were recorded in both the on- and off-zone modes, the latter were used primarily in the analyses due to its inherent increased sensitivity to the surface.[14] (Results presented here were obtained from analyses of a 14-member through-focal series.)

In the transmission geometry, electrons interact with the sample and carry information about the crystal potential into the image; this information transfer is, however, affected by the aberrations in the imaging system, and the recording and digitization processes. For samples tilted off the crystal zone axis, a simple linear-imaging theory[15,16] in combination with a weak-object approximation can be used to satisfactorily explain the HREM data. The intensity at each point, $I(r)$, can be expressed as

$$I(r) = 1 + \sigma t \int \{[A(u) \cos \chi(u) + B(u) \times \sin \chi(u)]E(u) + \eta(u)\} \exp(2\pi i u r) du , \quad (1)$$

where $A(u)$ and $B(u)$ are the real and imaginary parts of the crystal potential, $\eta(u)$ the background noise due to the statistics of the recording process, t the thickness and σ the interaction constant which depends on the microscope operating voltage. $\chi(u)$ and $E(u)$ denote the coherent and incoherent aberrations in the imaging system respectively, at each spatial frequency u in reciprocal space. Reconstruction of the wave exiting the sample, and thus the crystal potential, requires the removal of these aberration parameters.

One of the problems with gathering data in the off-zone condition is that the signal is small and noise becomes very important. As the first step, the images were enhanced by reducing the noise using a parametric Wiener filter approach described elsewhere.[17] Figure 2 demonstrates the result: a montage of the same region in a HREM image, prior

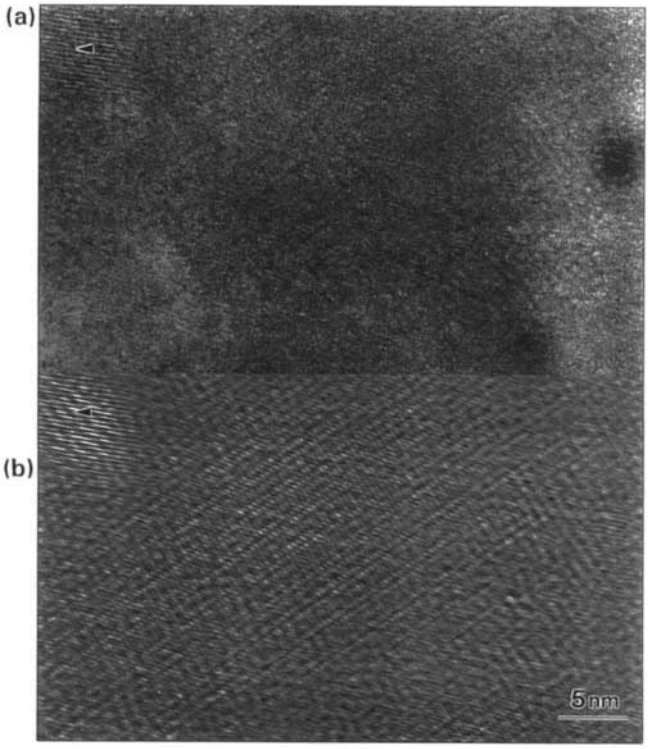

Fig. 2. Noise removal using a parametric Wiener filter.[17] (a) The prefiltered image with a particle arrowed for reference. (b) The noise-filtered image with the same arrowed particle demonstrating the efficacy of the technique.

to, and after the application of the filter. Signal-to-noise enhancement by a factor of about 6 is typically obtained.[17] This noise-filtered image shows stripes with a periodicity of nearly 1.92 nm, i.e., five times the spacing between the (110) planes in bulk silicon.

Extraction of the envelope term from these noise-corrected images was performed using an envelope-weighted parametric Wiener filter.[18] Figure 3 shows one such image at a defocus of 94 nm (where Schertzer defocus is 56 nm), corrected for both the envelope and noise contributions, and demonstrates the inhomogeneities in the stripe periodicity (which would give rise to the streaks in the diffraction patterns). Heavy directionality is also seen in the form of line features running at 45° to the rows; the origin of these will be described later.

Power spectra of such noise- and envelope-corrected images were subjected to a least-squares minimization process[18] to approximately invert for the crystal exit wave. The imaginary component of

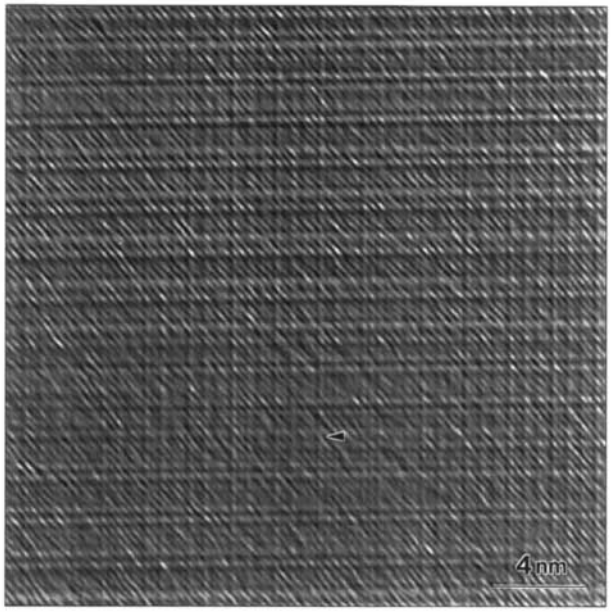

Fig. 3. An envelope-corrected image recorded at a defocus of 94 nm, showing the inhomogeneities in the reconstruction (arrowed) which would be responsible for the streaks in Fig. 1.

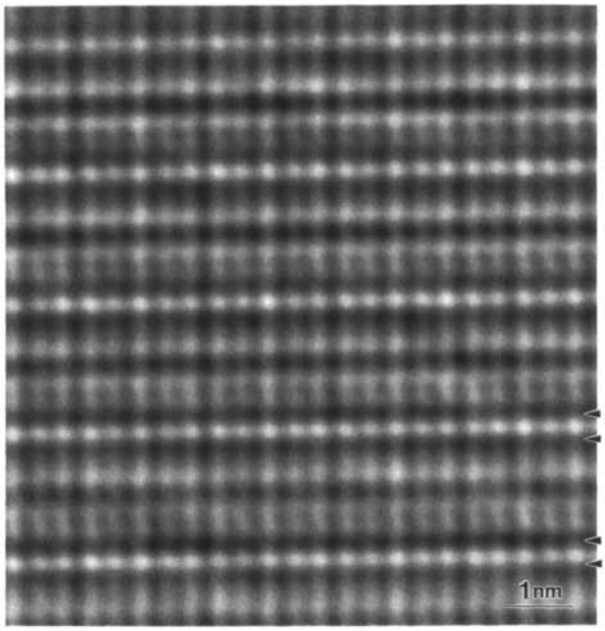

Fig. 4. The imaginary component of the exit wave reconstructed for an image recorded at a defocus of 118 nm. Pairs of high-contrast rows shown by the arrows are spaced 0.576 nm apart and are lined with Au atoms constituting the trench in the STM study.[10]

the exit wave reconstructed using this approach, for an image recorded at a defocus of 118 nm, is shown in Fig. 4. (Due to inaccuracies in the estimation of the microscope aberration parameters, the features in the reconstructed wave can only be interpreted in a qualitative sense; the envelope-filtered images, e.g., Fig. 3, on the other hand can be interpreted more accurately.[18])

4. Data Analysis

We will now develop a structure model using the diffraction and imaging data described in the previous section coupled with numerical simulations and the published STM results.[10] The correct atomic model for the surface must satisfactorily explain the features seen in the TED patterns and also be consistent with HREM data. Starting with the HREM data in Fig. 4, there are pairs of higher contrast rows spaced 0.576 nm, i.e., 1.5α, apart. These can be directly identified as arising due to Au, which scatters much more strongly than Si. The next issue is to register these atoms in the STM structure of *stripes* and *trenches*.

Since the inter-row spacing, which incidentally corresponds to twice the spacing between the (110) planes of pure Au, is higher than that between the (110) planes in bulk Si, these rows cannot form part of the stripe (where compression is reported), and would instead line the trench. The Au rows would therefore sit in subsurface layers, i.e., either the second, third, or fourth layer, where the outer surface is defined as the first layer.

4.1. *The trench*

The missing surface row in the STM structure model implies that the row directly bonded to it, i.e., in the second layer, could either be present or is also missing (this row is termed MSSL for missing surface second layer). This MSSL row along with the two second layer rows directly bonded to the outer rows of the stripe (termed ORSL for outer row second layer) constitute the two available locations for the Au atoms in this layer in the trench. Similarly, the third layer rows bonded to both the MSSL and one of the ORSL rows, and the fourth layer rows bonded to these third layer rows constitute the only possible sites for Au atoms in the trench in the respective layers.

Au atoms were allowed to sit in substitutional sites in these layers and the surface stripe was assumed to comprise purely silicon with the outer rows displaced towards the center, following the STM study.[10] (This compression is also consistent with the structure model obtained from this study, as will be discussed later.) Diffraction patterns were calculated for these four models of the trench, and the stripe using a pseudokinematical approach, i.e., for no tilt, and for a single-unit-cell thickness along the beam direction. Only a single domain of the reconstruction was used.

Visual fitting of these patterns against the experimentally recorded ones revealed that the second row positions could be completely ruled out since the 1,6/5 spots were extremely weak in comparison to the other reconstruction spots. (The 1,6/5 spots were used to test out the different models since they were consistently very strong.) On the other hand, patterns simulated for models with Au in the third or fourth layer positions described above, resulted in intensities several orders of magnitude higher in these spots. However, the intensities were similar for both the third and fourth layer Au models. Further, in contrast to the experimental patterns, the intensity value of these spots was identical to that of the 1,7/5 spots.

We therefore now have a partial structure for the trench with two Au rows in the third or fourth layers. There are, however, other details in the HREM images as well as those observed in STM that need to be explained, i.e., the *stripes* in the latter.

4.2. *The stripe*

Since the STM study reports a periodic arrangement of A- and B-type features on the stripe in a 5×3 cell, Au atoms were assumed to sit in substitutional sites corresponding to these (following the STM schematic, Au substituting for the A-type features were displaced parallel to the stripe; nondisplaced positions were also tested).

Starting off with the purely substitutional positions for Au atoms on both the stripes and the trenches, many different permutations of these locations were tested. The main two are: (a) Au atoms (irrespective of their position along the beam direction) substitute for Si directly, sit atop a bulk Si atom, or sit at interstitial locations; (b) the spacing

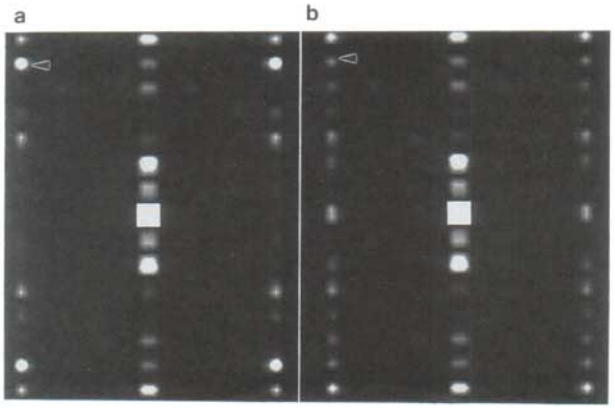

Fig. 5. Montage of diffraction patterns simulated for Au atoms sitting in substitutional sites in (a) the third layer and (b) the fourth layer in the bulk. Au atoms on the surface replace the B-type features in the schematic of the 5×3 cell.[10] The 1,6/5 type spots in the patterns are arrowed for reference.

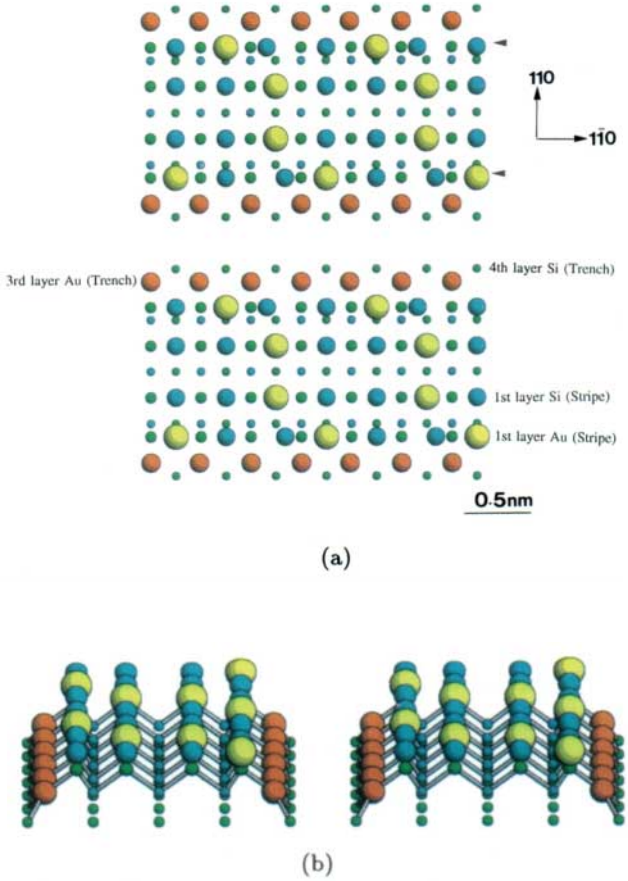

Fig. 6. (a) Top view and (b) perspective view schematic of the 5×3 cell used in simulation of the diffraction pattern in Fig. 5(a). Pairs of Au rows spaced 0.576 nm apart line the trench and four Au atoms sit in locations of the B-type features of the STM schematic;[10] note the surface layer compression of 16.7%.

between the Si rows directly bonded to the Au atoms in the trench could either be the bulk silicon separation value, i.e., 1α, or the value of the Au inter-row separation in the trench, i.e, 1.5α.

4.3. *The* 5×3 *cell*

On testing these stripe–trench combinations, it became apparent that the intensity of the 1,6/5 spots was highly sensitive to both the concentration and arrangement of the Au atoms, e.g., putting in Au atoms on the stripe resulted in a dramatic increase in the intensity of the 1,6/5 type spots (relative to the 1,7/5 and other reconstruction spots) as compared to the ones which had the Au atoms only in the trenches, as described in the earlier section. Further, it emerged that for either structure on the stripe (i.e., Au for A- or B-type features), the trench with Au atoms substituting for Si sites in the third layer and fourth layer Si atoms staying in bulk positions best explained the experimental data.

This is demonstrated in Fig. 5 which shows a montage of the TED patterns simulated for the two different locations for Au atoms along the beam direction, i.e., third and fourth layer substitutional sites (Au atoms substitute for the B-type features on the stripe), against Fig. 1. Figure 6 shows the real-space structure [top view in (a) and a perspective view in (b)] corresponding to the diffraction pattern in Fig. 5(a). If the Au atoms were to substitute for the A-type features in Fig. 6 instead, only an increase in the intensity of the 1,6/5 spots would be observed. In conclusion, a 5×3 cell alone cannot explain the strong intensity of the A-type spot pairs in Fig. 1.

4.4. *The* $\sqrt{26} \times 3$ *cell*

Using the $\sqrt{26} \times 3$ surface cell instead, the spot pairs were seen to lie on the reciprocal mesh corresponding to the four domains of this cell in real space. Figures 7(a) and 7(b) show two of these domains, labeled A and B respectively. A 90° rotation of these domains, e.g., across a single-layer high-step

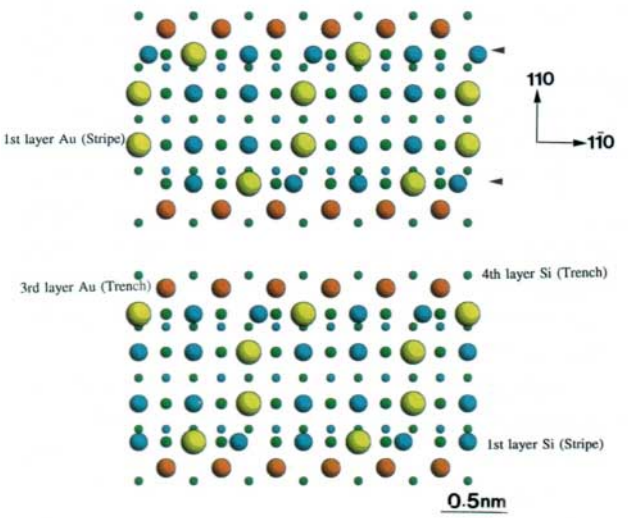

(a)

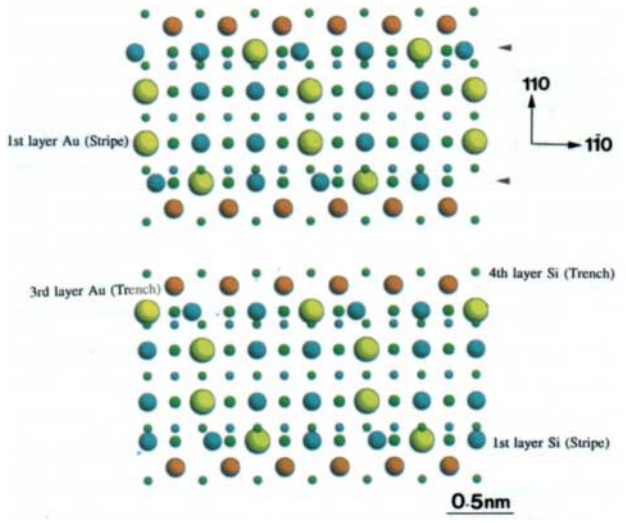

(b)

Fig. 7. (a) Schematic of the top view of the A-type domain of the $\sqrt{26} \times 3$ surface cell. Note the phase slip between adjacent stripes; Au rows line the trench and also substitute for B-type features in the STM schematic.[10] (b) Schematic of the top view of the B-type domain of the $\sqrt{26} \times 3$ surface cell. This domain is related to the domain in Fig. 7(a) by a mirror reflection.

boundary, would result in the other two, which we label as C and D respectively. Figure 8 is a schematic of Fig. 1, with letters A–D identifying the $\sqrt{26} \times 3$ reconstruction domains described above.

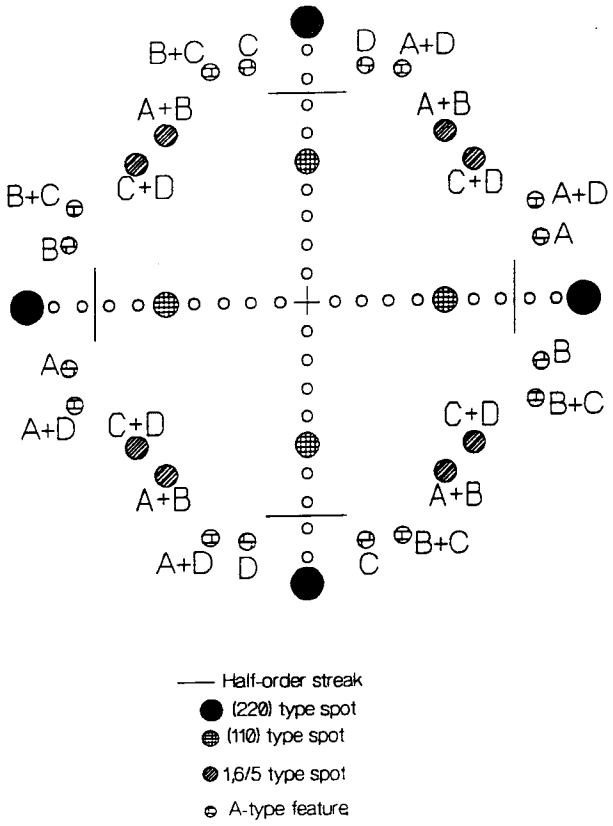

Fig. 8. Schematic of the diffraction pattern in Fig. 1, with the letters A and B indicating the contribution of the corresponding domains in Fig. 7; C and D represent domains obtained by rotating the A- and B-type domains in Fig. 7 by 90° (across a single-layer high step).

It should be noted that both the 5×3 or $\sqrt{26} \times 3$ geometries gave similar intensities for the 1,6/5 type spots implying that a mixed surface phase of the two structures as suggested by the STM study is possible. Since the models have to satisfactorily explain HREM data, the latter were used as a means to check the consistency.

4.5. *The consistency check*

Forward calculation of the HREM images was carried out for each of these models and the simulated images were compared against the envelope-corrected images for the corresponding defocus settings (e.g., Fig. 3). Such image comparisons clearly revealed a preference for the model of the stripe in which Au atoms substituted for the four B-type features and

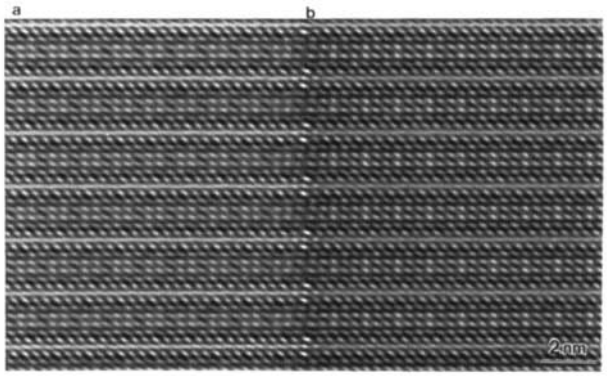

Fig. 9. Montage of HREM images simulated for the 5×3 cell, (a) with Au distribution on the stripe as in Fig. 6 and (b) with Au and Si interchanging stripe positions shown in Fig. 6. The directionality in the images arise due to anisotropy in the beam convergence in the simulations.

Si atoms for the other eight A-type features for these reasons: (a) interchanging the number of Au and Si atoms resulted in very strong contrast in the simulated images, which did not agree well with experimental data. Figure 9 shows images simulated for the two cases to illustrate this point (an anisotropic beam convergence term is assumed in the calculations, corresponding to the beam drift observed in the imaging process, and results in the directionality at 45° to the Au rows, similar to that seen in Fig. 4; (b) a total of ten Au atoms in the surface cell (four in the surface layer and six in the two rows in the third layer in the trench) would result in a fractional coverage of 0.67 ML per surface unit, in good agreement with the value of 0.7 ML predicted by XPS.[10]

It should be noted that we have assumed that the outermost rows move towards the center of the stripe based on STM data. The inter-Au row spacing of 1.5α represents an expansion relative to the bulk Si positions. Translating this to the outer rows on the surface, the resultant spacing between the four Si surface rows would be 2.5α rather than 3α. The associated surface layer compression of 16.7% is in good agreement with the 17% value reported in the STM study.[10]

5. Discussion

The behavior of Au on clean Si(100) surfaces, both at room temperature, and on annealing can be explained on the basis of a stress-relief-mediated mechanism. This behavior is directly related to the inherent nature of the clean Si(100)-(2 × 1) surface. It is well known that the Si(100)-(2 × 1) surface is under a strong tensile stress parallel to the dimer bond.[19] The tensile stress results because the dimerization favors compressive substrate strain parallel to the dimer bond; however, a rigid bulk lattice places the surface under a strong tensile stress,[20] and each atom involved in the dimerization still has an unsaturated dangling bond.

Au deposition at room temperature results in the transition of the clean 2×1 structure back to the ideal bulk-like 1 × 1 structure and can be attributed to the saturation of this dangling bond by a deposited Au atom. The STM study[8] revealed the saturation coverage for this surface to be 1 ML of Au (and reported a layer-by-layer growth for values up to 3 ML). However, the phase map[6] suggests that the 1 × 1 surface structure continues to exist at coverages exceeding this value; in fact, a weak silicide ring is reported to be detectable only at 3-nm Au deposit thickness. The excess Au (above the saturation value) could thus be accommodated either on the surface itself or in the bulk. In case of accommodation in the Si bulk lattice, the bulk material would be strained in the Au-containing region due to the differences in the radii of the two species.

Annealing the system would provide a mechanism for the release of this strain via rearrangement of atoms, both on the surface and in the bulk. The final surface structure resulting from this process, i.e., the Si(100)–Au-(5 × 3) phase, is thermodynamically favored based on both the phase map[6] and other studies,[5,10] and can be completely described on the basis of the surface stripe, the subsurface trench, and the single missing row of atoms, see Figs. 6 and 7. This missing surface row can be visualized as a "surface dislocation". The term was first defined to describe the formation process for the Si(111)-(7 × 7) surface,[21] and was recently invoked to explain the structure model for the Si(111)–Au-(5 × 2) structure.[13]

While the current investigation does not provide data on the actual origin of the dislocation, the latter has to be directly related to the subsurface Au row expansion. Such an expansion would place a compressive stress on the surrounding silicon layers in the rigid bulk lattice. Translation of this stress to

the surface layer would result in the compression of the outer two rows on the stripe, of magnitude equal to that of the expansion of the subsurface rows.

A few points of caution about the model:

(i) The structure models proposed in the study (i.e., 5×3 and $\sqrt{26} \times 3$) assume an ordered arrangement of pure Au and Si atoms. The presence of a gold–silicide compound can however not be ruled out, and in fact, small amounts might even be present, although their contribution to the features in the TED patterns is unknown.

(ii) Further, since transmission data are highly sensitive to positions in the plane orthogonal to the incident beam, the intensity of the 1,6/5 spot changes with small displacements in the x–y plane. The current structure results therefore, are intended to only serve as a qualitative description of the atom distribution. More rigorous quantitative calculations (involving R-factor and χ^2 tests) would be required to predict the exact atomic structure.

(iii) Finally, the relative insensitivity of these data to the positions along the beam direction (z) implies that techniques such as x-ray standing wave and LEED would therefore be better suited for determining these locations.

Acknowledgments

We are grateful to the Air Force Office of Scientific Research for having supported this work on grant number AFOSR-90-0045.

References

1. K. Hricovini, J. E. Bonnet, B. Carrière, J. P. Deville, M. Hanbücken, and G. LeLay, *Surf. Sci.* **211/212**, 630 (1989).
2. M. Hanbücken, Z. Imam, J. J. Métois, and G. LeLay, *Surf. Sci.* **162**, 628 (1985).
3. A. Hiraki, *Surf. Sci.* **168**, 74 (1986).
4. T. Narusawa, K. Kinoshita, W. M. Gibson, and A. Hiraki, *J. Vac. Sci. Technol.* **18**, 872 (1981).
5. K. Oura, Y. Makino, and T. Hanawa, *Jpn. J. Appl. Phys.* **15**, 737 (1976).
6. K. Oura and T. Hanawa, *Surf. Sci.* **82**, 202 (1979).
7. A. K. Green and E. Bauer, *Surf. Sci.* **103**, L127 (1981).
8. X. F. Lin and J. Nogami, *J. Vac. Sci. Technol.* **B12**, 2090 (1994).
9. Z. H. Lu, T. K. Sham, and P. R. Norton, *Solid State Commun.* **85**, 957 (1993).
10. X. F. Lin, K. J. Wan, J. C. Glueckstein, and J. Nogami, *Phys. Rev.* **B47**, 3671 (1993).
11. J. E. Bonevich and L. D. Marks, *Microscopy* **22**, 95 (1992).
12. G. Jayaram, P. Xu, and L. D. Marks, *Phys. Rev. Lett.* **71**, 3489 (1993).
13. L. D. Marks and R. Plass, *Phys. Rev. Lett.*, in press.
14. L. D. Marks, P. Xu, and D. N. Dunn, *Surf. Sci.* **294**, 322 (1993).
15. J. C. H. Spence, *Experimental High Resolution Electron Microscopy* (Oxford University Press, Inc., New York, 1988).
16. P. Buseck, J. Cowley, and L. Eyring, *High Resolution Transmission Electron Microscopy* (Oxford University Press, Inc., New York, 1988).
17. L. D. Marks, *Ultramicroscopy*, in press.
18. L. D. Marks, in preparation.
19. R. D. Meade and D. Vanderbilt, *The Structure of Surfaces III*, eds. S. Y. Tong, M. A. Van Hove, K. Takayanagi, and X. D. Xie, *Springer Series in Surface Sciences* Vol. 24 (Springer-Verlag Berlin: Heidelberg, 1990), p. 4.
20. H. Sato and K. Yagi, *J. Phys.: Condens. Matter* **5**, 2095 (1993).
21. P. M. Petroff and R. J. Wilson, *Phys. Rev. Lett.* **51**, 199 (1983).